First-principles study of the SiN$_x$/TiN(001) interface

Tobias Marten,[*] Björn Alling, Eyvaz I. Isaev, Hans Lind, Ferenc Tasnádi, Lars Hultman, and Igor A. Abrikosov

Department of Physics, Chemistry and Biology (IFM), Linköping University, SE-581 83 Linköping, Sweden
(Received 31 August 2011; revised manuscript received 27 January 2012; published 8 March 2012)

The structure of the SiN$_x$ tissue phase in superhard TiN/SiN$_x$ nanocomposites has been debated in the literature. We present a theoretical investigation of the possibility of crystalline and coherent (001) interfaces that satisfies the two necessary criteria, stability with respect to lattice vibrations as well as to variations in stoichiometry. It is found that one monolayer of Si tetrahedrally coordinated by N in a B3-like geometry embedded between B1-TiN(001) surfaces is both dynamically stable and thermodynamically stable with respect to vacancy formation. However, with increasing layer thickness the B3-type structure becomes unstable with respect to Si vacancy formation. Instead we suggest that a tetragonal D0$_{22}$-like order of Si vacancies can stabilize the interface. These structures are in line with the experimental findings of the crystalline tissue phase which has coherent interfaces with TiN.

I. INTRODUCTION

Superhard nanocomposites (nc) are an important class of materials with a large potential as wear-protective coatings in industrial metal working processes such as drilling, cutting, and milling. In particular TiN-SiN$_x$ has become a model system in the field,[1,2] which may be extended to more complex multicomponent nitrides by, for example, Al and Cr addition in TiAlSiN[3,4] and CrAlSiN.[5] Due to the extreme immiscibility of Si$_3$N$_4$ in TiN, solid solutions are typically not formed to a considerable extent during vapor deposition thin film growth. Instead an nc is formed with small TiN grains and a SiN$_x$ tissue phase at the grain boundaries. The increased hardness of nc-TiN/SiN$_x$, as compared to pure TiN films is qualitatively attributed to two distinct effects. First the small crystallite size of TiN grains prevents the nucleation and motion of dislocations. Second, the tissue phase of SiN$_x$ provides strong intergranular bonds, which prevents grain boundary sliding, whose detrimental effect has been observed in other nanocrystaline systems.[6] Unfortunately, a quantitative description of the hardening mechanism of the SiN$_x$ phase is still not established. Nevertheless, in order to understand the superhardening phenomenon and the mechanism beyond the limiting factors it is of high importance to study the structure of the SiN$_x$ phase. This point has been debated in the literature. First, the SiN$_x$ phase was considered to be amorphous,[7] later reformulated as "x-ray amorphous".[8] However, contemporary and subsequent experiments showed that a crystalline phase up to six monolayers (ML) of SiN$_x$ could be stabilized in an apparent epitaxial manner between TiN(001) interfaces.[9–11] On the theoretical side, Hao *et al.* studied the TiN/SiN$_x$/TiN(111) interfaces and suggested different SiN$_x$ geometries as a function of the nitrogen chemical potential and oxygen contaminations.[12–14] Motivated by the experimental findings of apparent epitaxial (001) interfaces, a number of theoretical studies then considered the properties of a hypothetical rocksalt (B1) structure of SiN, both in bulk[15] and as a single monolayer between TiN slabs.[16]

Later a theoretical study showed that the B1 phase of SiN is dynamically unstable with respect to lattice vibrations in bulk.[17] The related cubic, but tetrahedrally coordinated zincblende (B3) phase was much lower in energy but also dynamically unstable. The electronic origin of these instabilities was suggested to be related to the unfavorable Si$_1$N$_1$ stoichiometry. Due to the inherent dynamical instability, these phases cannot exist in the bulk or as thick layers. Instead two fcc-related pseudo-B3 Si$_3$N$_4$ phases derived from a L1$_2$- or D0$_{22}$-type distribution of Si vacancies, with lattice spacings close to TiN, were shown to be dynamically stable and were suggested as possible candidates to explain the experiments.[17]

However, it was argued[18,19] that a single monolayer of stochiometric B1 SiN could be stabilized between TiN(001) slabs by distortion of the Si-N bonds. In those cases, the limiting factor of the hardness was discussed in terms of Friedel oscillations of the electronic charge density near the interface.

Later Marten *et al.*[20] showed that distortions of the bonds had a stabilizing effect on the lattice dynamics, but the phonon spectra still contained weak imaginary frequencies. Even though the structure might be stabilized dynamically by thermal effects, it was shown that both the (001) and the (111) interfaces are thermodynamically unstable with respect to spontaneous formation of Si vacancies in the lattice. The conclusion was that the isostructural B1 TiN/SiN interfaces with a Si$_1$N$_1$ stoichiometry are unlikely to be present in experimental samples.

In this work, we build upon the knowledge gained from previous experimental and theoretical investigations and suggest possible atomic arrangements of the tissue phase in the apparent epitaxial TiN/SiN$_x$/TiN(001) interfaces. We have used the B3-related structures suggested in Ref. 17 as possible metastable structures of bulk SiN$_x$ as a starting point for generating candidate interface structures with 1 and 3 ML of Si. We check their stability against atomic relaxations, collective lattice vibrations, and with respect to fluctuations in the stoichiometry. Furthermore we report the electronic structure of these interfaces.

II. METHODOLOGY

All simulations were carried out in the framework of the density functional theory. The geometrical optimization of the multilayers and electronic structure problem were solved using the projector augmented wave method (PAW)[21,22] implemented in the *ab initio* simulation package VASP.[23,24] The calculations of phonon dispersions were done using the linear response method[25] utilized in QUANTUM-ESPRESSO.[26] In this

case, *ab initio* pseudopotentials by Vanderbilt[27] were used to describe the interactions among the valence electrons and the ions. The used pseudopotentials have previously been shown to give excellent agreement with both experiments and other theoretical methods considering phonon and bulk parameters (see Refs. [28] and [29]). Electronic exchange-correlation effects are described by means of the generalized gradient approximation (GGA) parametrized according to Perdew *et al.*.[30] Plane-wave energy cutoffs of 400 eV and 40 Ry were used in the VASP and QUANTUM-ESPRESSO calculations, respectively. Monkhorst-Pack grids were used for the *k*-space sampling with a density of $7 \times 7 \times 3$ *k* points for the larger in-plane slabs, $11 \times 7 \times 3$ for the intermediate-sized slabs, and 15x15x5 for the the small slabs. The bulk phases were calculated with a mesh of $21 \times 21 \times 21$ *k* points. Force constants for phonon calculations were obtained using a $4 \times 4 \times 2$ q-point mesh.

The interfaces are modeled by two B1 TiN(001) slabs each consisting of four layers. The slabs are coupled together by the SiN$_x$ tissue phase, which in the case of a 1-ML-thick interface consist of two nitrogen layers and one silicon layer and in the case of a 3-ML-thick interface consist of four nitrogen layers and three silicon layers. The structures are drawn in Figs. [1] and [2(a)] for the case of 1-ML- and 3-ML-thick interfaces, respectively. We are interested in investigating the relevance of the dynamically stable bulk SiN$_x$ phases presented in Ref. [17] for the interface structures observed as epitaxial with continued lattice fringes in, for example, Ref. [9]. For this aim, as a starting geometry we let them connect smoothly to the TiN slabs in both ends by allowing the nitrogen atoms continue the fcc sublattice of N in TiN. Thus, we have excluded the possibility of a relative in-plane relaxation between the TiN slabs above and below the SiN$_x$ phase. Different in-plane sizes of the supercells were used in order to simulate different vacancy concentrations and vacancy-vacancy separations. In the smaller cell a vacancy concentration of one out of four (1/4) was introduced in the silicon plane with a vacancy separation of $\sqrt{2}a_0$ before structural relaxations. In the larger cell we simulate a vacancy concentration of one out of eight (1/8) and the corresponding vacancy separation is $2a_0$. Here a_0 denotes the calculated lattice parameter of the conventional TiN cubic cell, 4.255 Å. In all calculations, the studied property was converged with respect to the *k*-points sampling as well as the energy cutoff of the plane-wave basis set and obtained at fully optimized geometries.

III. RESULTS

A. TiN/1ML-SiN$_x$ interface

Figure [1] shows the geometry considered for the interface with a single Si monolayer. Due to the tetrahedral coordination between Si and N in B3 SiN, the (001) interface is polar, in opposite to the B1 structure. Since experimental observations show a distinct increase in N to (Ti + Si) ratio when the content of Si is increased (e.g., Ref. [31]), and that typical growth condition are nitrogenrich enough to yield stoichiometric TiN,[1] we chose to study the nitrogen terminated interfaces. The findings in Refs. [9–11], that is, the indication of a tendency for epitaxial (001) interfaces in the case of thin SiN$_x$ layers, motivate us to let the nitrogen fcc sublattice merge smoothly
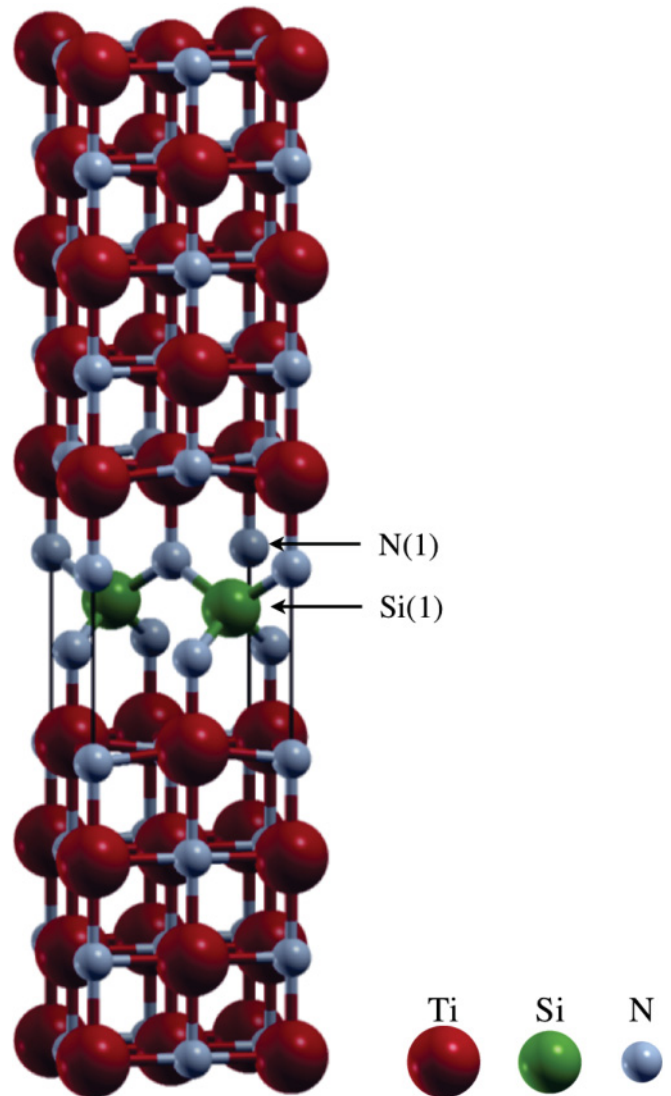
FIG. 1. (Color online) Structure of the one-monolayer B3 coordinated SiN interface. Si(1) and N(1) denote the inequivalent positions at the interface. See text for further discussion.

to that of nitrogen in TiN. The stability of this geometry was subsequently tested with respect to static displacements and relaxations, collective lattice vibrations, and vacancy formation.

In order to allow for relative displacements of the Si and N atoms in the interface, we perform structural optimizations using different displaced initial coordinates of the Si atoms. In all those cases, the Si atoms relax into the corresponding ideal in-plane B3 positions although the direction normal to the interface is somewhat changed. This contrasts to the case of a B1 structure monolayer where the energy is lowered significantly upon in-plane distortion of Si atoms.[19,20] The mean interplanar distances of the structure given in Fig. [1] are (in Å): TiN(bottom layer)–2.13–TiN–2.13–TiN–2.19–TiN–2.06–N–0.93–Si(central layer).

Before entering the discussion of the vacancy formation energies, we note that the suggested interface structure of Fig. [1] has a nitrogen rich 1:2 Si-to-N stoichiometry originating from the polar character of the (001) surface in the B3

(a)

(b)
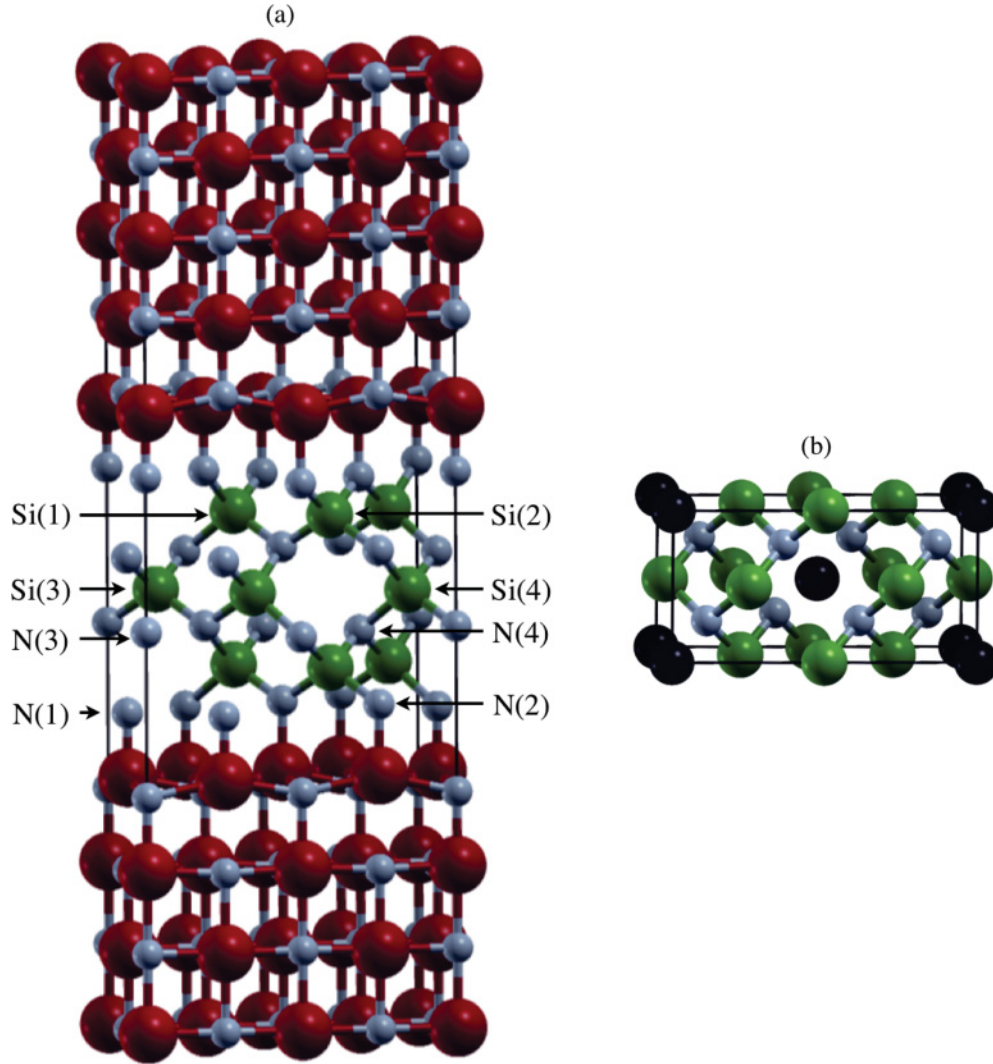
FIG. 2. (Color online) (a) The $D0_{22}$-type interface. (b) The bulk unit cell of $B3$-$D0_{22}$-Si_3N_4. Silicon vacancies are indicated by black spheres. The color code introduced in Fig. 1 is adopted. Si(1), . . . , Si(4) and N(1), . . . , N(4) denote the inequivalent silicon and nitrogen positions at the interface. See text for further discussion.

structure. We stress the difference to a B1 monolayer that would have a 1:1 Si-to-N stoichiometry. As stated above, during typical physical vapor deposition growth the films form under nitrogen-rich conditions. However, to have the full picture, we show formation energies for Si vacancies also with respect to the Si chemical potential taken from N-poor conditions and from bulk Si. Formation energies of a single Si vacancy has been calculated according to

$$E_v^{Si} = E_{slab}(-1Si) - E_{slab} + \mu_{Si}, \quad (1)$$

where $E_{slab}(-1Si)$ and E_{slab} are the total energies of the system with and without a silicon vacancy, respectively, and our choice of the silicon chemical potential, μ_{Si}, follows the discussion by Hao et al.:[12,14]

$$\mu_{Si} = \begin{cases} \frac{1}{3}E(i_3N_4) - \frac{2}{3}E(N_2) & (N-rich) \\ \frac{1}{2}E(TiSi_2) - \frac{1}{2}E(Ti) & (N-poor) \\ E(Si) & (bulk\ Si). \end{cases}$$

Total energies, per formula units, of the involving systems have been derived from the β phase of Si_3N_4, the N_2 molecule, the base-centered orthorhombic c49 crystal structure of $TiSi_2$, the hcp phase of Ti, and at last the diamond structure of Si. Our calculated structural parameters of the compounds agree with earlier theoretical and experimental works, for example, Refs. 13 and 32–34. According to Hao et al.[12,14] the use of bulk Si as chemical potential is not relevant, regardless of the nitrogen chemical potential, as it never becomes lowest in energy. Yet, it could be useful in the analysis of vacancy formation energies for its simplicity and transparency and for comparison reasons as it provides an upper limit of μ_{Si}.

The silicon vacancy formation energies obtained for the single Si monolayer interface are summarized in Table I. As seen from the table the calculated formation energies of a single silicon vacancy is strongly positive, 4.8–5.5 eV under nitrogen-rich conditions. This means that it is not energetically favorable to release a silicon atom from the interface and let it react with the surroundings. In addition, the nitrogen vacancy formation energy, $E_v^N = E_{slab}(-1N) - E_{slab} + \frac{1}{2}E(N_2)$,

TABLE I. Silicon vacancy formation energy, E_v^{Si} in eV, for the 1-ML-thick B3 coordinated SiN interface shown in Fig. 1. E_v^{Si} is computed according to Eq. (1). Column two and three, that is, 1/4 and 1/8, respectively, represent the ratio of silicon vacancies within the layer.

μ_{Si}	1/4	1/8
N-rich	5.5	4.8
N-poor	7.3	6.6
Bulk Si	8.1	7.4

is positive, 2.8–2.9 eV at vacancy concentrations 1/4 and 1/8, respectively. Here we have used $\mu_N = \frac{1}{2} E(N_2)$, corresponding to the excessive nitrogen in the system. This finding is in clear contrast to the findings of negative formation energies for the B1 stoichiometric monolayers.[20] The explanation is most probably that the interface layer of Fig. 1, as compared to a B1 layer, has both a more favorable coordination geometry of the Si atoms (tetrahedral), as well as coordination number (4 N atoms). The fact that also the nitrogen vacancy formation energy is large and positive shows that the interface is not too over-stoichiometric in nitrogen. Actually this value of nitrogen vacancy formation energy is higher than 2.41 eV found in Ref. 35 for a nitrogen vacancy in pure TiN.

To check the stability of the 1-ML-thick interface geometry with respect to collective atomic vibrations, *ab initio* phonon calculations have been performed. Figure 3 shows the phonon dispersion relations along the high symmetry directions in the Brillioun zone. Clearly, all branches are real and there are no signs of imaginary frequencies found for the B1 monolayer.[20] Thus, we conclude that this interface geometry is indeed a likely candidate for single Si ML embedded in TiN(001).

The electronic structure of the interfaces are of interest not only because they determine structural and dynamical stabilities, but also for electrical and transport properties of the nc-systems. It is well established that TiN is a good electrical conductor with a finite electronic density of states at the Fermi level. Bulk Si_3N_4 on the other hand is an insulator. The calculated electronic density of states for bulk
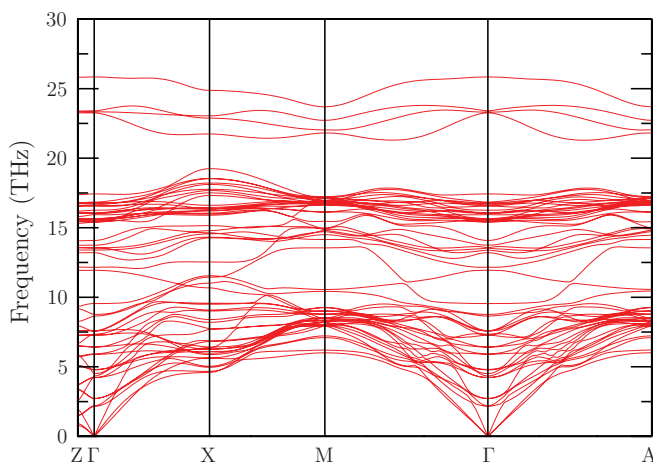
FIG. 3. (Color online) Calculated phonon spectrum for the 1-ML-thick B3 coordinated SiN interface shown in Fig. 1.
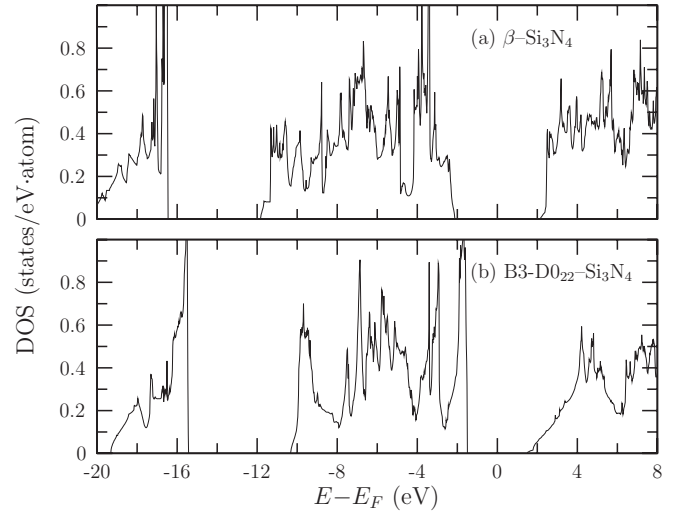
FIG. 4. Electron density of states for bulk (a) β-Si_3N_4 and (b) B3-D0$_{22}$–Si_3N_4.

β and B3-D0$_{22}$ phases of Si_3N_4 are shown in Fig. 4. The unit cell of the latter phase is drawn in Fig. 2(b). The semiconductor character of both those systems in bulk are seen, and calculated band gaps are 4.24 eV in β-Si_3N_4 and 2.98 eV in B3-D0$_{22}$–Si_3N_4. We note that GGA calculations typically underestimate experimentally measured band gaps. We now turn to the electronic structure of the 1-ML-thick interface. Figure 5 shows the site-projected electronic density of states, that is, the partial DOS, on the Si and N atoms of the interface indicated with arrows in Fig. 1. The electronic spectra for Si and N atoms of the 1-ML-thick interface show some similarities with the B3-based B3-D0$_{22}$ bulk Si_3N_4. However, there is no distinct band gap and the interface is barely metallic with a peak in state density at and above E_F.
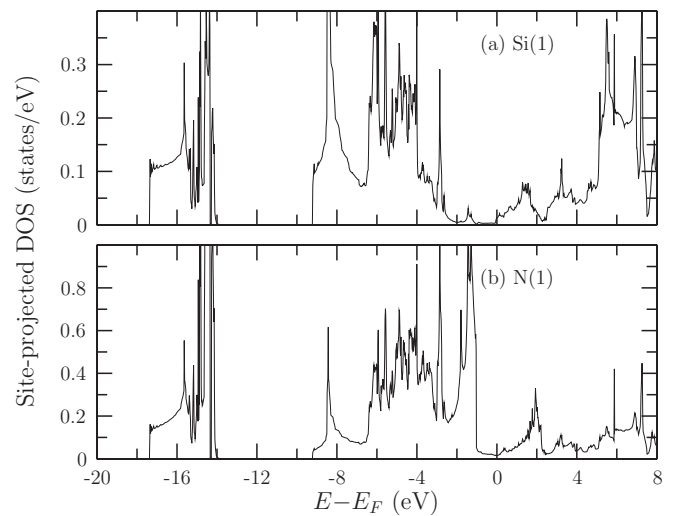
FIG. 5. Site-projected density of states for the 1-ML-thick B3 coordinated interface. Si(1) and N(1) denote the silicon and nitrogen positions defined in Fig. 1.

TABLE II. Silicon vacancy formation energy E_v^{Si}, calculated according to Eq. (1), for the 3-ML-thick B3 coordinated interface. The numbers in brackets [i.e., $(\cdots)$] refer to the Si layers closest to the TiN matrix whereas the other numbers refer to the central layer of Si. Columns two and three show the result for in-plane Si vacancy concentration 1/4 and 1/8, respectively.

μ_{Si}	1/4	1/8
N-rich	−7.4 (−2.7)	−7.0 (−4.2)
N-poor	−5.7 (−0.9)	−5.2 (−2.4)
Bulk Si	−4.8 (−0.1)	−4.4 (−1.6)

B. TiN/3ML-SiN$_x$ interface

As shown above the B3-type geometry of the 1-ML-thick interface is stable both with respect to formation of vacancies as well as to lattice vibrations. This is of importance for understanding nc-TiN/SiN$_x$ films with a Si content corresponding to 1-ML coverage of the TiN grains. However, the experimental findings show the possibility of an apparent epitaxy up to about 6 ML. Thus, one should consider also thicker interfaces. In the present study we do that by simulating a system with 3 ML of Si in a B3-based interface. We start with considering the formation energy of Si vacancies, summarized in Table II. In contrast to the 1-ML case, the silicon vacancy formation energies are strongly *negative*. At the relevant nitrogen-rich conditions we find for a vacancy fraction of one out of four Si atoms $E_v^{Si} = -7.4$ eV for the middle layer and $E_v^{Si} = -2.7$ eV for the Si layers closest to the interface with TiN. With the lower vacancy concentration, one out of eight Si atoms, $E_v^{Si} = -7.0$ eV for the middle and $E_v^{Si} = -4.2$ eV for the Si layers closest to the TiN slab. Thus, with increasing layer thickness the B3-type structure becomes considerably unstable with respect to change in stoichiometry. An explanation of the instability can be found in the local 1:1 stoichiometric ratio between Si and N that appears at the center of the interface with increasing layer thickness. This stoichiometry is definitely unfavorable, to the extent that bulk B3-SiN is dynamically unstable as shown in Ref. 17.

Thus, we are led to consider if the introduction of Si vacancies could stabilize thicker SiN$_x$ layers like it was shown to be the case in bulk Si$_3$N$_4$.[17] We do so by introducing an interface built from the D0$_{22}$-type ordering of vacancies on the B3 lattice. This geometry is shown in Fig. 2(a) while the unit cell of the bulk B3-D0$_{22}$–Si$_3$N$_4$ is shown for clarity in Fig. 2(b). In this geometry, all Si atoms have four N nearest neighbors while the atoms of the two central N planes all have the ideal three silicon atom coordination. The N atoms closest to the TiN slabs each have one Ti and either one or two Si neighbors. The mean interplanar distances of the structure given in Fig. 2 are (in Å): TiN(bottom layer)–2.13–TiN–2.17–TiN–2.25–TiN–2.02–N–1.05–Si–1.02–N–1.03–Si(central layer).

Table III shows the calculated formation energies of Si vacancies at different positions defined in Fig. 2(a) in the B3-D0$_{22}$-like 3-ML-thick interface. All values are now positive. However, the formation energy of a vacancy at the nitrogen site close to the TiN slab with just one Si neighbor is barely positive. We find $E_v^N = 0.1$, 2.2, 3.2, and 2.3 eV for nitrogen vacancies at positions N(1), ..., N(4), respectively.

TABLE III. Vacancy formation energy E_v^{Si} for the 3-ML-thick D0$_{22}$-type interface. Si(1), ..., Si(4) denote the inequivalent silicon positions defined in Fig. 2. 1/3 refers to the in-plane Si vacancy concentration.

μ_{Si}	1/3			
	Si(1)	Si(2)	Si(3)	Si(4)
N-rich	4.5	7.6	4.6	6.8
N-poor	6.2	9.4	6.3	8.6
Bulk Si	7.1	10.2	7.2	9.4

The numbers are obtained at an in-plane N vacancy fraction of 1/4.

The dynamical stability of the 3-ML-thick system with vacancies has not been studied explicitly due to huge computational costs. However, we note that the B3-D0$_{22}$ structure of Si$_3$N$_4$ from which the interface geometry is derived is dynamically stable in bulk.[17] Furthermore, the presence of the TiN(001) interfaces should give a stabilizing effect as was found for the 1-ML case above and for the isostructural B1
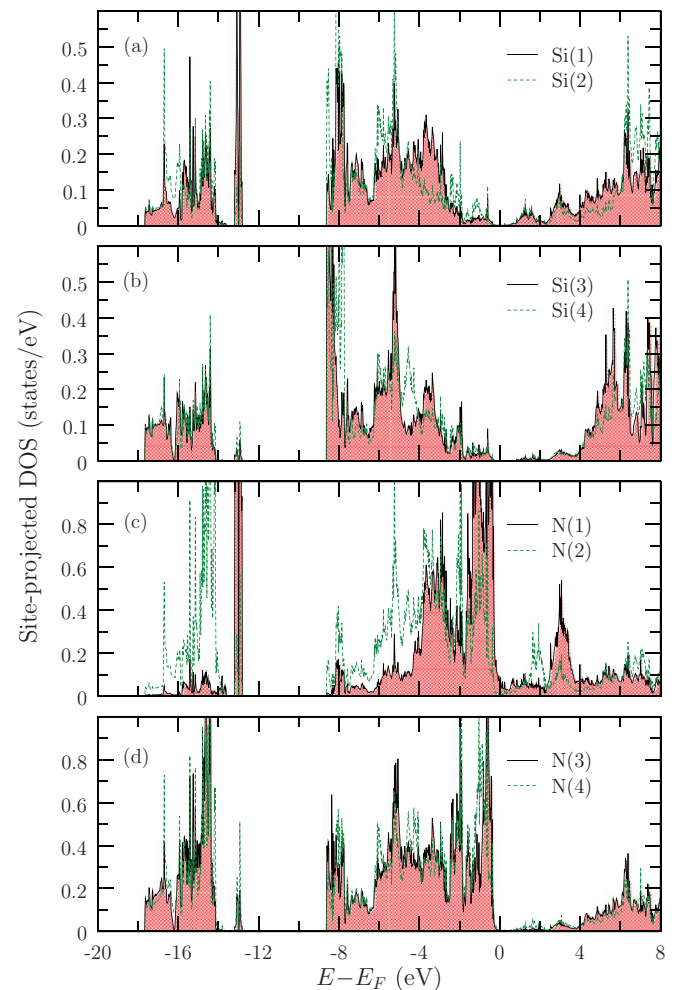
FIG. 6. (Color online) Site-projected density of states for the 3-ML-thick interface with D0$_{22}$-type ordering of silicon vacancies. Si(1), ..., Si(4) and N(1), ..., N(4) denote the inequivalent silicon and nitrogen positions defined in Fig. 2.

interfaces in Ref. 20. However, deeper investigations of this issue would be valuable in the future.

The calculated site-projected electronic density of states for the 3-ML-thick interface with $D0_{22}$-type ordering of silicon vacancies are shown in Fig. 6. The top two panels show the DOS projected to the Si sites while the lower two display the N site-projected DOS. The DOS of the Si atoms and the N atoms in layers in the middle of the interface (numbers 3 and 4) show a striking similarity with the DOS of bulk $B3-D0_{22}-Si_3N_4$ presented in Fig. 4(b) with the development of a band gap at the Fermi level, although much more narrow as compared to the bulk case. On the other hand, the N layers closest to the TiN interface retain a metallic character.

IV. CONCLUSIONS

We report results of first-principles density functional theory study of the structure of SiN_x tissue phase in TiN/SiN_x superhard nanocomposites. We have studied the stability of several candidate crystalline structures of SiN_x at the (001) interface with TiN against atomic relaxations, collective lattice vibrations, and with respect to fluctuations in the stoichiometry. As regards the 1-ML-thick SiN_x interface we find that a B3-derived interface with a tetrahedral coordination between Si and N is stable to both silicon and nitrogen vacancies. Moreover, the phonon dispersion relation shows no peculiarities, in contrast to ideally stoichiometric single ML with B1 coordination. The 1-ML-thick B3 interface has a nitrogen-rich stoichiometry and avoids the unfavorable 1:1 Si-to-N ratio of the B1 ML. The tetrahedral coordination geometry of the Si atoms is also preferred over the octahedral coordination of the B1 structure. Thus, we conclude that this

interface geometry is a likely candidate for real existing single Si ML embedded in TiN(001).

One important observation is that the 1-ML-thick interface is metallic and has a nonzero electronic DOS at and above the Fermi level. However, there is a distinct pseudogap below the Fermi level.

With increased SiN_x layer thickness, achieved by repetition of the B3 structural units, the local stoichiometry of the central layers reaches the unfavorable 1:1 ratio. Already at 3-ML thickness we found the B3-derived interface to be thermodynamically unstable against formation of Si vacancies, manifested by their strongly negative formation energies.

We then investigated a 3-ML interface geometry based on the introduction of Si vacancies in line with a $D0_{22}$-type ordering on the B3 lattice. Indeed, this stabilizes the system against spontaneous formation of more silicon vacancies. On the other hand, the vacancy formation energy for one of the nitrogen atoms is almost zero. This suggests that even more complex geometries, possibly based on alternative types of Si and N coordination, ordering of Si vacancies, as well as the details of the matching between the TiN(001) slab and thicker SiN_x layers should be further investigated.

ACKNOWLEDGMENTS

*tobias.marten@liu.se

[1] S. Veprek, M. G. J. Veprek-Heijman, P. Karvankova, and J. Prochazka, Thin Solid Films **476**, 1 (2005).

[2] S. Veprek, J. Nanosci. Nanotechnol. **11**, 14 (2011).

[3] S. Veprek, H. D. Männling, M. Jilek, and P. Holubar, Mater. Sci. Eng. A **366**, 202 (2004).

[4] A. Flink, J. Andersson, B. Alling, R. Daniel, J. Sjölén, L. Karlsson, and L. Hultman, Thin Solid Films **517**, 714 (2008).

[5] J. Soldán, J. Neidhardt, B. Sartory, R. Kaindl, R. Cerstvý, P. Mayrhofer, R. Tessadri, P. Polcik, M. Lechthaler, and C. Mitterer, Surf. Coat. Technol. **202**, 3555 (2008).

[6] J. Schiotz, F. D. Di Tolla, and K. W. Jacobsen, Nature (London) **391**, 561 (1998).

[7] S. Veprek and S. Reiprich, Thin Solid Films **268**, 64 (1995).

[8] S. Veprek, High Press. Res. **26**, 119 (2006).

[9] L. Hultman, J. Bareño, A. Flink, H. Söderberg, K. Larsson, V. Petrova, M. Odén, J. E. Greene, and I. Petrov, Phys. Rev. B **75**, 155437 (2007).

[10] H. Söderberg, M. Odén, J. M. Molina-Aldareguia, and L. Hultman, J. Appl. Phys. **97**, 114327 (2005).

[11] H. Söderberg, M. Odén, A. Flink, J. Birch, P. O. A. Persson, M. Beckers, and L. Hultman, J. Mater. Res. **22**, 3255 (2007).

[12] S. Hao, B. Delley, S. Veprek, and C. Stampfl, Phys. Rev. Lett. **97**, 086102 (2006).

[13] S. Hao, B. Delley, and C. Stampfl, Phys. Rev. B **74**, 035402 (2006).

[14] S. Hao, B. Delley, and C. Stampfl, Phys. Rev. B **74**, 035424 (2006).

[15] R. F. Zhang, S. H. Sheng, and S. Veprek, Appl. Phys. Lett. **90**, 191903 (2007).

[16] S. Veprek, A. S. Argon, and R. F. Zhang, Philos. Mag. Lett. **87**, 955 (2007).

[17] B. Alling, E. I. Isaev, A. Flink, L. Hultman, and I. A. Abrikosov, Phys. Rev. B **78**, 132103 (2008).

[18] R. F. Zhang, A. S. Argon, and S. Veprek, Phys. Rev. Lett. **102**, 015503 (2009).

[19] R. F. Zhang, A. S. Argon, and S. Veprek, Phys. Rev. B **79**, 245426 (2009).

[20] T. Marten, E. I. Isaev, B. Alling, L. Hultman, and I. A. Abrikosov, Phys. Rev. B **81**, 212102 (2010).

[21] P. E. Blöchl, Phys. Rev. B **50**, 17953 (1994).

[22] G. Kresse and D. Joubert, Phys. Rev. B **59**, 1758 (1999).

[23] G. Kresse and J. Furthmüller, Phys. Rev. B **54**, 11169 (1996).

[24] G. Kresse and J. Hafner, Phys. Rev. B **49**, 14251 (1994).

[25]S. Baroni, S. de Gironcoli, A. Dal Corso, and P. Giannozzi, Rev. Mod. Phys. **73**, 515 (2001).

[26]P. Giannozzi, S. Baroni, N. Bonini, M. Calandra, R. Car, C. Cavazzoni, D. Ceresoli, G. L. Chiarotti, M. Cococcioni, I. Dabo, A. D. Corso, S. de Gironcoli, S. Fabris, G. Fratesi, R. Gebauer, U. Gerstmann, C. Gougoussis, A. Kokalj, M. Lazzeri, L. Martin-Samos, N. Marzari, F. Mauri, R. Mazzarello, S. Paolini, A. Pasquarello, L. Paulatto, C. Sbraccia, S. Scandolo, G. Sclauzero, A. P. Seitsonen, A. Smogunov, P. Umari, and R. M. Wentzcovitch, J. Phys. Condens. Matter **21**, 395502 (2009).

[27]D. Vanderbilt, Phys. Rev. B **41**, 7892 (1990).

[28]E. I. Isaev, R. Ahuja, S. I. Simak, A. I. Lichtenstein, Y. K. Vekilov, B. Johansson, and I. A. Abrikosov, Phys. Rev. B **72**, 064515 (2005).

[29]E. I. Isaev, S. I. Simak, I. A. Abrikosov, R. Ahuja, Y. K. Vekilov, M. I. Katsnelson, A. I. Lichtenstein, and B. Johansson, J. Appl. Phys. **101**, 123519 (2007).

[30]J. P. Perdew, K. Burke, and M. Ernzerhof, Phys. Rev. Lett. **77**, 3865 (1996).

[31]A. Flink, M. Beckers, J. Sjölen, T. Larsson, S. Braun, L. Karlsson, and L. Hultman, J. Mater. Res. **24**, 2483 (2009).

[32]C. Stampfl, W. Mannstadt, R. Asahi, and A. J. Freeman, Phys. Rev. B **63**, 155106 (2001).

[33]R. Zhang and S. Veprek, Thin Solid Films **516**, 2264 (2008).

[34]O. Borgen and H. M. Seip, Acta Chem. Scand. **15**, 1789 (1961).

[35]L. Tsetseris, N. Kalfagiannis, S. Logothetidis, and S. T. Pantelides, Phys. Rev. B **76**, 224107 (2007).